Rare Metal Materials and Engineering
Volume 54, Issue 1, January 2025
Available online at www.rmme.ac.cn

Science Press

Cite this article as: Chong Yufan, Du Zhaoxin, Gong Tianhao, et al. Effects of Cerium-Rich Rare Earth and Al-Ti-B Composite Addition on Microstructure and Mechanical Properties of Al-Mg-Si Alloys[J]. Rare Metal Materials and Engineering, 2025, 54(01): 50-61. DOI: 10.12442/j.issn.1002-185X.20240427.

ARTICLE

Effects of Cerium-Rich Rare Earth and Al-Ti-B Composite Addition on Microstructure and Mechanical Properties of Al-Mg-Si Alloys

Chong Yufan[1], Du Zhaoxin[1], Gong Tianhao[1], Sun Baoan[2], Pan Zheru[1], Qi Lele[1], Xie Chengcheng[1], Cheng Jun[3]

[1] School of Materials Science and Engineering, Inner Mongolia University of Technology, Hohhot 010051, China; [2] Institute of Physics, Chinese Academy of Sciences, Beijing 100190, China; [3] Northwest Institute for Nonferrous Metal Research, Xi'an 710016, China

Abstract: Modification of 6061 aluminum alloy was conducted through composite addition of cerium-rich rare earths and Al-Ti-B. Results show that the composite addition of Al-Ti-B and Ce/La element at a specific ratio notably promotes the refinement of the alloy's grains. Ce and La elements are combined with Si and other elements to form rare earth phases, improving the morphology and distribution of precipitates and mitigating the adverse effects of β-Fe phases on the microstructure and mechanical properties of alloy. However, excessive rare earth content poses challenges; it not only leads to a decrease in Mg-Si strengthening phase by binding with Si but also promotes the formation of larger or numerous rare earth phases that may act as initiation points for cracks, thereby impeding the improvement of the structure and performance of alloy. The composite addition of cerium-rich rare earths and Al-Ti-B not only preserves the strength of the alloy but also significantly enhances the plasticity of the 6061 as-cast alloy. At a composite addition ratio of Al-Ti-B:RE=2:1, the newly developed 6061-RE aluminum alloy exhibits increased average elongation by 50% and 45% in its as-cast and homogenized states, respectively, compared to the baseline 6061 alloy, facilitating subsequent deformation processing. After solution treatment at 540 °C for 1 h and aging at 180 °C for 5 h, the average ultimate tensile strength and yield strength of 6061-RE alloys reach 313.2 and 283.1 MPa, increased by 12.3% and 14.5% compared with those of the original alloy, respectively, and the average elongation is improved by 41%.

Key words: rare earth alloy; Al-Mg-Si alloy; cerium-rich rare earth; mechanical property; microstructure

Al-Mg-Si series alloys are increasingly employed in automotive components as alternatives to traditional steel, offering substantial benefits in mass reduction[1–2]. The 6061 aluminum alloy, characterized by excellent formability, mechanical robustness and corrosion resistance, is predominantly used for manufacturing wheel hubs, body panels and battery trays[3]. However, challenges persist in enhancing the comprehensive mechanical performance of the 6061 aluminum alloy while simultaneously reducing production costs and meeting market demands. Grain refinement and microalloying are proven strategies to improve the strength and toughness of aluminum alloys. The traditional refiner, Al-Ti-B, effectively facilitates grain refinement in these alloys, primarily through the action of $TiAl_3$ and TiB_2. Despite their efficacy, issues such as the aggregation and precipitation of species like Ti_2B, along with the adverse effects of elements such as Cr and Zr, can significantly undermine these benefits[4–6]. Additionally, although rare earth elements play a crucial role in refining grains and microalloying during metal solidification, thereby improving secondary phases, their excessive application can degrade the integrity of the original alloy structure[7–14]. Moreover, the high

Received date: July 15, 2024
Foundation item: Subproject of Inner Mongolia Autonomous Region Key Research and Development and Achievement Transformation Plan Project (2023YFDZ0064, 2023KJHZ0020, 2022YFDZ0097); Natural Science Foundation of Inner Mongolia Autonomous Region of China (2022QN05040); Basic Research Funds for Directly Affiliated Universities in Inner Mongolia Autonomous Region (JY20220093); Program for Young Talents of Science and Technology in Universities of Inner Mongolia Autonomous Region (NJYT24008)
Corresponding author: Du Zhaoxin, Ph. D., Professor, School of Materials Science and Engineering, Inner Mongolia University of Technology, Hohhot 010051, P. R. China, Tel: 0086-471-6575752, E-mail: duzhaoxin@163.com

costs associated with rare earths like Sc, Gd and Er often hinder their widespread implementation in large-scale alloy production.

La and Ce elements can refine the grain structure and ameliorate the morphology and distribution of Fe-rich phases β-Fe and α-Fe, as well as the principal strengthening phase Mg_2Si, in Al-Mg-Si series aluminum alloys, thereby enhancing the material properties while maintaining lower costs[15–18]. To achieve improvements in material performance and cost reduction, and to address the diminishing effectiveness of the Al-Ti-B refiner, traditional refiners such as Al-Ti-B and Al-Ti-C are usually integrated with rare earth elements. This approach for aluminum alloy modification encompasses two main strategies: firstly, the development of a novel intermediate alloy refiner, Al-Ti-B-RE, which is added to the aluminum alloy matrix to increase heterogeneous nucleation sites and to facilitate grain refinement; secondly, the research focuses on the aluminum alloy matrix itself, foregoing the production of the Al-Ti-B-RE intermediate alloy. Instead, Al-Ti-B or Al-Ti-C along with rare earth elements like Ce and La are directly incorporated into the aluminum alloy matrix for modification[19–22]. Ce and La elements are adjacent in atomic number, and their chemical properties exhibit minimal disparity. However, the Ce element exerts a more pronounced purifying influence on Fe and Si impurities within the aluminum matrix, facilitating the straightforward formation of Al-Fe-Si-Ce compounds within the aluminum matrix. In contrast, the La element is more susceptible to the formation of solid solution in the aluminum matrix[23–24]. Additionally, some studies have indicated that the combined addition of Ce and La has a more pronounced effect on the strength enhancement of Al-Mg-Si alloys than the individual addition of La or the combined addition of La and Er[25]. This streamlined process combines the advantages of grain refinement and microalloying, although the current research on composite modification lacks in alloy composition design and mechanistic understanding. This study focused on investigating the compositional strategies and elucidating the mechanisms, especially the direct composite addition of cerium-rich rare earths and Al-Ti-B, and is poised to advance the development and application of cost-effective high-performance aluminum alloys. The Al-Mg-Si alloy is categorized as a heat-treatable aluminum alloy, i. e., the thermomechanical treatments of solution and aging are pivotal in enhancing its strength and other mechanical properties. Predominantly, the Mg_2Si phase, along with its age-related precipitates and evolution forms, such as the β'' and β' Mg-Si phases, serves as the principal strengthening phases[26–29]. Thus, these features attract considerable attention from researchers exploring the microstructure and performance attributes of the Al-Mg-Si alloy, which reflects its critical role in optimizing the alloy's mechanical characteristics.

In this study, traditional grain refiner Al-Ti-B was combined with cost-effective cerium-rich rare earths for direct composite addition into the 6061 aluminum alloy matrix for modification. A comparative analysis was designed involving seven distinct alloy composition. The modified and unmodified 6061 aluminum alloys were characterized by optical microscope (OM), scanning electron microscope (SEM), transmission electron microscope (TEM) and differential scanning calorimetry (DSC). This comprehensive characterization facilitates the elucidation of the effects of the combined addition of Al-Ti-B and cerium-rich rare earths on microstructure and macroscopic mechanical properties of the Al-Mg-Si alloy. The preliminary findings suggest that this innovative modification approach achieves superior enhancements in properties of 6061 aluminum alloy.

1 Experiment

This study involved experiments with eight distinct alloy groups, and commercially available 6061 aluminum alloy was used as the base matrix, whose composition is shown in Table 1. Commercially sourced Al-Ti-B grain refiner and Al-20Ce/La master alloy were employed as modification additives, where the Ce:La ratio in the Al-20Ce/La alloy was 65:35. The composition designs for the seven modified groups of 6061 alloy are outlined in Table 2, where Z0 represents the baseline 6061 alloy remelted under identical melting conditions, and Z1 to Z7 represent alloys melted with varying concentrations of additives. Each group of alloy ingots was obtained via vacuum induction melting followed by casting. Subsequent treatments involved homogenization of the as-cast alloys in a box furnace at 550 °C for 6 h, solution treatment at 540 °C for 1 h and aging treatments at 160 and 180 °C for 5 h.

In this experiment, samples for microstructural observation were uniformly excised from the same region of the casting ingots to maintain consistent conditions and to mitigate any potential variations in solidification rates that may affect the microstructure. These samples were then polished by an advanced metallurgical polishing machine and etched by Keller's reagent for 22 s. Anodization was conducted in 1.8% fluoroboric acid solution, with the power supply set to 20 V

Table 1 Chemical composition of 6061 aluminum alloy (wt%)

Mg	Si	Fe	Zn	Cu	Mn	Ti	Cr	Al
0.76	0.65	0.52	0.25	0.29	0.15	0.035	0.05	Bal.

Table 2 Compositional design of 6061 aluminum alloy modified by composite additive of different ratios with total amount of 0.3wt%

Alloy	Ce/La/wt%	Al-Ti-B/wt%	Al-Ti-B:Re
Z0	0	0	-
Z1	0	0.30	3:0
Z2	0.075	0.225	3:1
Z3	0.10	0.20	2:1
Z4	0.15	0.15	1:1
Z5	0.20	0.10	1:2
Z6	0.225	0.075	1:3
Z7	0.30	0	0:3

and current ranging from 0.3 A to 0.5 A. Microstructural assessments of the alloys, including grain size, surface morphology and precipitate phases, were conducted by Axio Imager Zeiss optical microscope (OM), Leica DM4 P polarized light microscope and FEI-Quanta 650 FEG field emission environmental SEM. Further characterization of the precipitate phases' morphology, quantity and elemental composition was performed by TEM. Phase analysis was carried out on samples that had been mechanically polished and cleaned with alcohol, using the high-temperature X-ray diffractometer (XRD) in a measurement range of 2θ=20°–90°. Thermal properties of the samples were evaluated using the LABSYS evo high-low temperature simultaneous thermal analyzer of DSC, across a temperature range from 25 °C to 750 °C, with a uniform heating/cooling rate of 10 °C/min. Cylindrical tensile samples with a gauge length of 25 mm were machined by the DK7740 electrical discharge CNC wire-cut machine and a lathe. These samples were subjected to tensile testing at room temperature on an Instron 5980 dual-column floor-standing universal testing machine at stretching rate of 2 mm/min, and the results of three samples per set were averaged, as shown in Fig. 1. The experimental methodology incorporated a series of distinct heat treatment processes, outlined as follows. Initially, the homogenization heat treatment in the experiment involved maintaining the alloy samples at 550 °C for 6 h, followed by air cooling to room temperature. The solution heat treatment was conducted at 540 °C, at which the samples were maintained for 1 h before being quenched in water to room temperature. The aging process was subsequently performed at 180 °C, at which the alloy was maintained for 5 h followed by air cooling.

2 Results and Discussion

2.1 OM test

Polarized light microscope was employed to characterize the microstructures of eight groups of as-cast alloys after anodization, as depicted in Fig.2. Relative to the original 6061 alloy shown in Fig.2e, the grain sizes of the alloys modified with Al-Ti-B or cerium-rich rare earths are notably refined.

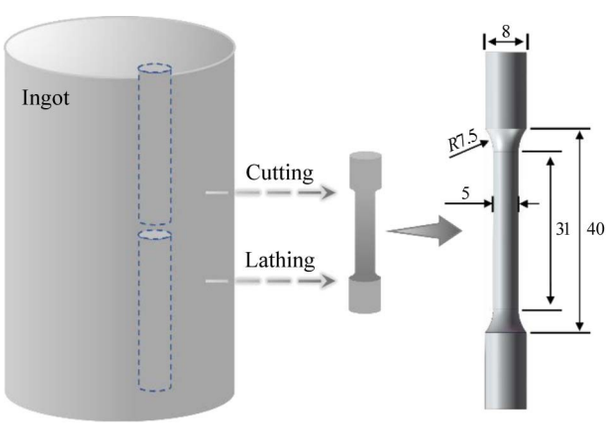

Fig.1 Location, shape and size of tensile sample used in experiment

This refinement can be attributed to two main mechanisms: firstly, the addition of Al-Ti-B, which promotes α-Al nucleation and grain refinement via the formation of TiB_2 and Al_3Ti particles, as supported by the dual nucleation theory; secondly, the addition of Ce and La rare earth elements, which increases compositional undercooling to promote dendritic crystal formation, enhances nucleation, and, as surfactant elements, slows down grain growth. When the composite addition ratio of Al-Ti-B to RE is 2:1, 1:1 and 1:3, the alloy grains are fine and uniform. However, at a ratio of 3:1, significant grain size heterogeneity is observed, potentially adversely affecting the mechanical properties of the alloy. After etching, the microstructures of the as-cast samples are observed, as shown in Fig.3. In the original 6061 alloy, many grains exceed 150 μm in length, but in alloys Z3, Z5 and Z6 with Al-Ti-B: RE ratios of 2:1, 1:2 and 1:3, respectively, multiple grains around 30 μm in length are observed within a 100 μm scale field, indicating significant grain refinement. Conversely, in alloy Z4 with Al-Ti-B:RE ratio of 1:1, a tooth-like pattern of small and large grains is interspersed. At the grain boundaries of each alloy group, dendritic and rod-like Fe-rich phases are present. These phases are coarser and more pronounced in the original 6061 alloy and the alloy containing higher content of Al-Ti-B. The addition of cerium-rich rare earths has a refining or microalloying effect on these Fe-rich phases. Regarding the intragranular particulate and dot-like precipitate phases, based on their size, they are identified as modified α-Fe phases and Mg-Si phases, rather than smaller heterogeneous nucleation sites such as Al_3Ti or Ti_2B[30–31]. Furthermore, a comprehensive analysis of Fig. 2 and Fig. 3 reveals that alloys with only 0.3wt% cerium-rich rare earths have relatively larger grains than other modified alloys. This observation can be attributed to the lack of Al-Ti-B to provide nucleation sites and increase in rare earth compound growth, which reduces the compositional undercooling effect at the solid/liquid interface due to increased rare earth content.

2.2 Mechanical property

Tensile mechanical properties of each group of as-cast alloys, homogenized alloys and those subjected to solution treatment at 540 °C for 1 h followed by artificial aging for 5 h were tested, and the results are illustrated in Fig.4. Initially, it is observed that the elongation of the alloys is generally declined, followed by an increase, and then subsequently decreases as the ratio of Al-Ti-B to rare earth elements increases. The pattern of strength variation is less distinct, which may be because the macroscopic mechanical properties of the alloys are influenced by the changes in microstructural grain size and the morphology, type and distribution of secondary phases induced by the addition of cerium-rich rare earths. Among the alloys, alloy Z2, with an Al-Ti-B:RE ratio of 3:1, displays a noticeable decline in both strength and ductility, ranking it as the lower performers in the group. This can be correlated with the significant grain size heterogeneity observed by OM and possible effect of the distribution of secondary phases. For the three conditions of the alloys studied, alloy Z3, with a composite addition ratio of Al-Ti-B

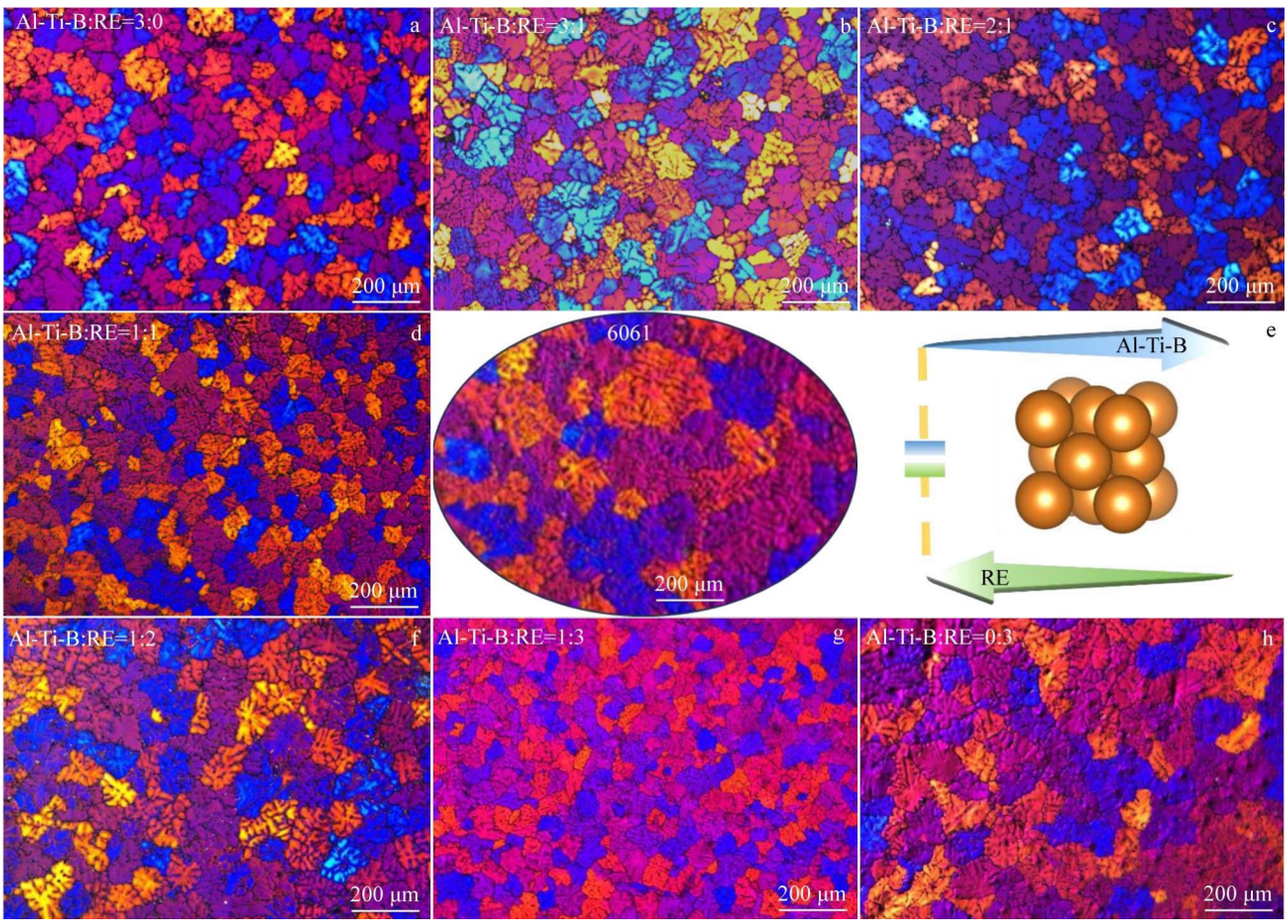

Fig.2 Polarized light microscope images of microstructure of as-cast alloy samples after anodization modified with different Al-Ti-B:RE ratios: (a) 3:0, (b) 3:1, (c) 2:1, (d) 1:1, (e) original 6061 alloy and its fcc structure, (f) 1:2, (g) 1:3, and (h) 0:3

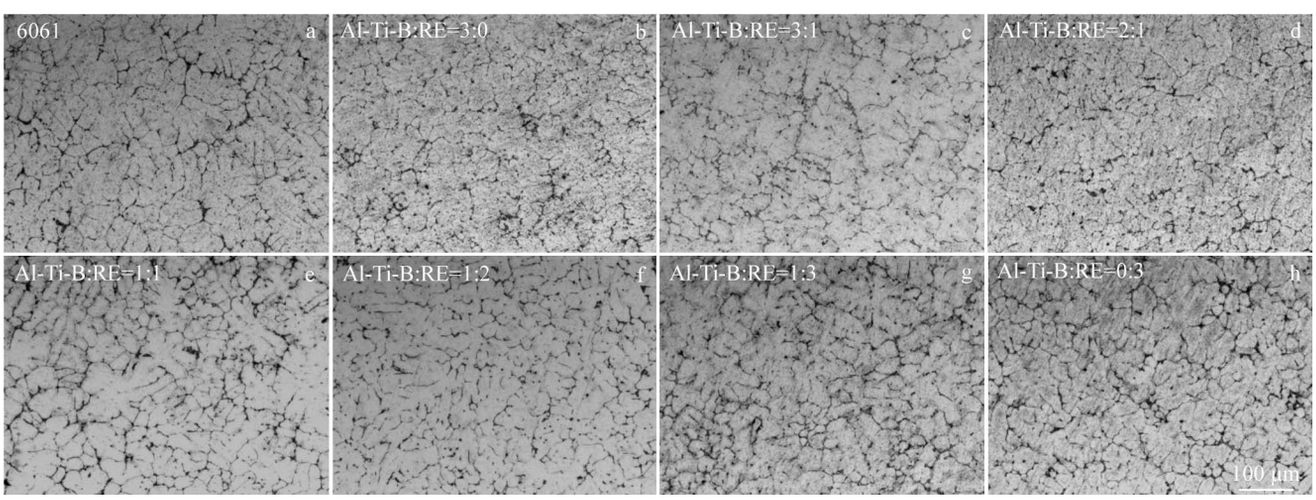

Fig.3 OM images of as-cast original 6061 alloy (a) and modified alloys with different Al-Ti-B:RE ratios (b–h): (b) 3:0, (c) 3:1, (d) 2:1, (e) 1:1, (f) 1:2, (g) 1:3, and (h) 0:3

to cerium-rich rare earths of 2:1, exhibits the best plasticity. The as-cast alloy Z3 has an average elongation of 13.8% (the maximum reaching up to 15.8%), while its yield strength and ultimate tensile strength remain 95.2 and 188.8 MPa, respectively, ranking it as the top performers in the group. After homogenization, the average elongation of alloy Z3 increases to 16.5%. After the solution and aging treatment, the alloy Z3 maintains an average elongation above 3%, with its average ultimate tensile strength reaching 313.2 MPa. The favorable plastic deformation capacity and strength levels of alloy Z3 create advantageous conditions for subsequent material processing, deformation and application.

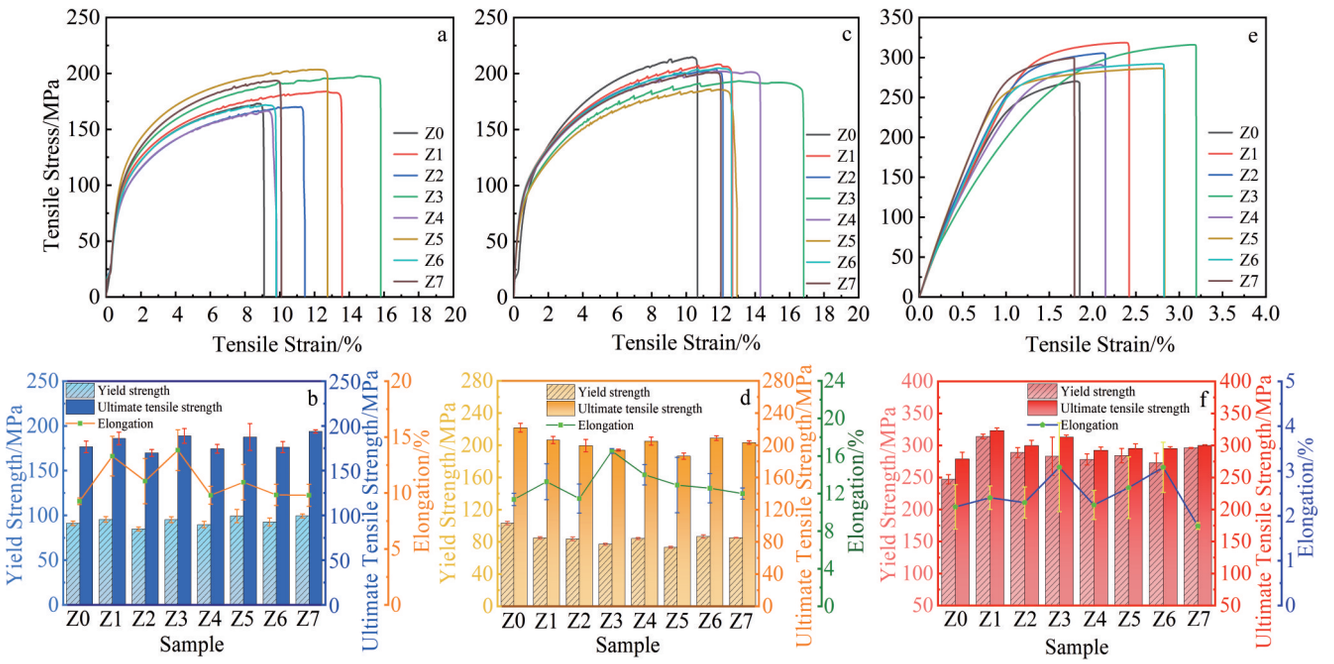

Fig.4 Tensile tress-tensile strain curves (a, c, e) and tensile mechanical properties (b, d, f) of eight groups of alloys in different states: (a–b) as-cast, (c–d) after homogenization heat treatment, and (e–f) after solid solution and aging treatment

2.3 DSC and XRD testing

DSC analysis was performed on the original 6061 aluminum alloy, alloys with individual additions of Al-Ti-B or cerium-rich rare earths and those modified with a composite addition, and the resulting curves are depicted in Fig. 5. Alloy solidification theory suggests that the nucleation undercooling of an alloy is the temperature difference between the liquidus temperature of the alloy and its nucleation temperature, which is closely related to the nucleation driving force during the solidification process. According to the melting curves of the alloys, there are no significant differences in the initial melting temperatures across the groups, indicating that the minor additions of Al-Ti-B or Ce and La elements have minimal impact on the alloy ' s melting process, and the liquidus temperatures remain basically unchanged. Therefore, changes in the nucleation temperatures of the alloys can be used to gauge variations in nucleation undercooling during solidification[32]. In the solidification curves, the pronounced peaks A and B are, according to phase diagram analysis, associated with the nucleation of α-Al and Fe-rich phases, respectively. The initial nucleation temperature of α-Al in the original 6061 aluminum alloy is 645 °C, which slightly increases to a range within 647 and 648 °C upon the addition of Al-Ti-B and rare earth elements, indicating a decrease in nucleation undercooling of α-Al with the addition of these additives. However, for the cerium-rich rare earths, once their addition content exceeds 0.1wt%, the nucleation undercooling of α-Al remains nearly constant, no longer changing with variations in the amount of rare earth added. Conversely, the nucleation undercooling of the Fe-rich phases increases with the addition of rare earth elements but also stabilizes once the addition content of cerium-rich rare earths exceeds 0.1wt%. With increasing the addition content of rare earth elements, the emergence of exothermic peak C likely corresponds to the formation of rare earth phases.

XRD patterns for the as-cast alloys are presented in Fig.6. It indicates pronounced diffraction peaks corresponding to aluminum across all alloys. Additionally, at a diffraction angle

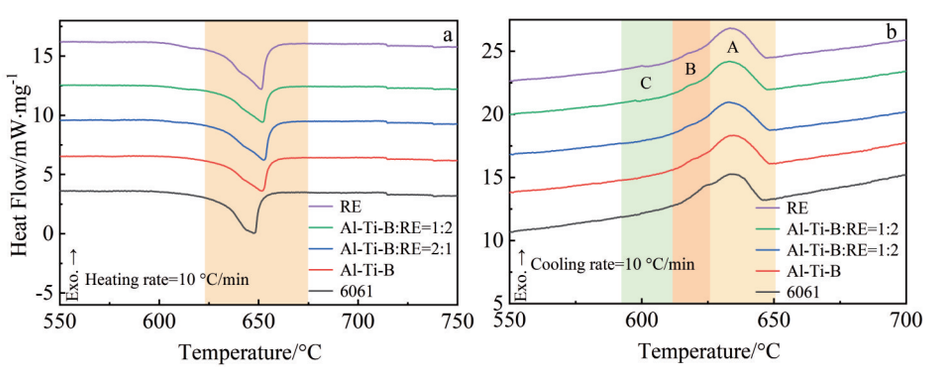

Fig.5 DSC curves of as-cast original 6061 alloy and modified alloys: (a) melting curves and (b) solidification curves

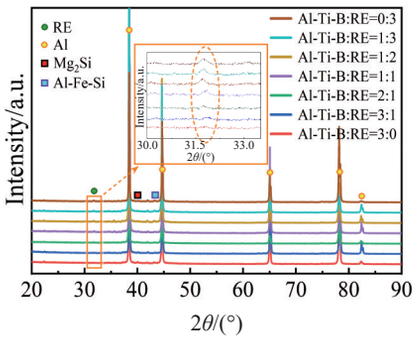

Fig.6 XRD patterns of modified as-cast alloys with different Al-Ti-B:RE ratios

of 40.2° , peaks corresponding to the strengthening phase Mg_2Si are evident. The position of the Mg_2Si peaks shows negligible shift with the introduction of rare earth elements, suggesting that these trace additions do not alter the crystal structure of the alloy. However, the intensity of the Mg_2Si peaks decreases with the incorporation of rare earth elements. This reduction is likely due to the formation of new rare earth phases with the silicon atoms in Mg_2Si, thereby diminishing the Mg_2Si content. Adjacent to the Mg_2Si peaks, diffraction peaks associated with Fe-rich phases are also observed, as referenced in previous studies[33–35]. It is particularly noteworthy that there is significant variation between spectra in diffraction angle range of 31° to 32° . The red spectrum line shown in Fig. 6 represents XRD pattern of alloy Z1, which only includes Al-Ti-B; this spectrum does not exhibit any peaks within the aforementioned diffraction angle range. However, with the addition of cerium-rich rare earths, new diffraction peaks appear, and the intensity of these peaks increases progressively with the proportion of rare earth elements increasing. Compared with standard diffraction patterns, these new peaks may be identified as Ce, $CeCu_2Si_2$ and $AlCe_3$, yet they do not coincide exactly. Some researchers have described similar peak positions as the phases such as $Al_{11}Ce_3$, $Al_{11}La_3$, $Al_{11}CeMg_6$ or La_5Si_3[18,25,36]. This study hypothesizes that these peaks indeed correspond to rare earth compounds containing Ce and La, likely in a transitional state before stabilizing. The variation in peak intensity suggests an increase in the content of rare earth compound that is proportional to the increase in rare earth element content. This provides evidence for the hypothesis that cerium-rich rare earths are not only concentrated at the alloy grain boundaries to enhance compositional undercooling and to promote grain refinement but also play a role in microalloying.

2.4 SEM and EDS analysis

To objectively observe and analyze the influence of varying additive ratios on the precipitate phases in 6061 aluminum alloy, SEM characterization at backscattered electron (BSE) mode was conducted on each group of as-cast samples. In Fig. 7, the original 6061 alloy (Z0) exhibits noticeable inhomogeneity in its as-cast microstructure, characterized by the presence of large-sized light gray Fe-rich phases continuously distributed in elongated rod-like and dendritic shape[18,37–39], with fewer dot-like and spherical precipitates. Upon the addition of Al-Ti-B to the 6061 aluminum alloy, as shown in Fig. 7b, the morphology of the Fe-rich phases remains basically unchanged, but their distribution becomes more dispersed. This dispersion is attributed to the fact that Fe-rich phases in 6061 alloys are predominantly located along grain boundaries. The introduction of Al-Ti-B leads to a noticeable refinement of the alloy grains, thus altering the overall distribution of these phases, without changing their intrinsic morphology or phase type. When Al-Ti-B is combined with cerium-rich rare earths in the 6061 aluminum alloy matrix, as depicted in Fig. 7c – 7g, the distribution of precipitates becomes more dispersed, and their specific morphologies also change: some elongated β -Fe phases reduce in size and lighten in color, and this trend becomes more obvious with the increased addition of rare earth elements. With Al-Ti-B:rare earths ratio of 1:1, larger regions devoid of precipitates appear in the alloy, but the Fe-rich phases are uneven in size. Additionally, bright white feather-like or flake-shaped inclusions appear at the edges or in the

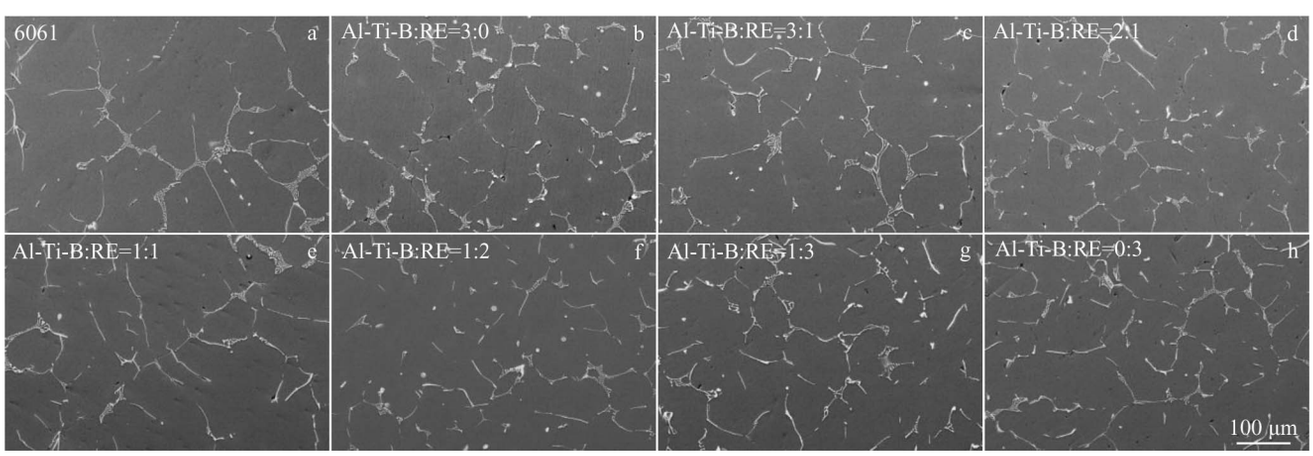

Fig.7 SEM-BSE images of as-cast original 6061 alloy (a) and modified alloys with different Al-Ti-B:RE ratios (b–h): (b) 3:0, (c) 3:1, (d) 2:1, (e) 1:1, (f) 1:2, (g) 1:3, and (h) 0:3

middle of the Fe-rich phases. The size and quantity of these bright white inclusions also increase as the proportion of rare earths increases. Based on the characteristic of BSE images, in which elements with higher atomic numbers appear lighter in color, it is inferred that these bright inclusions are likely rare earth phases[18,39–40].

To mitigate the effects of dendritic segregation and non-equilibrium phases, each group of as-cast aluminum alloys was subjected to homogenization treatment, resulting in a distribution pattern of precipitates similar to that observed in the as-cast state. As illustrated in Fig. 8f – 8h, alloys with composite additions and those with only rare earth additions more distinctly exhibit bright white, feather-like and flake-shaped suspected rare earth inclusions, which have increased size and become more sharply defined at the edges with higher rare earth content. From the perspective of the morphology, size and continuity of the Fe-rich phases, the composite addition of cerium-rich rare earths and Al-Ti-B effectively facilitates the shortening and spheroidization of the brittle β-Fe phase towards the α-Fe phase, with a more pronounced discontinuous and dispersed distribution. This transformation reduces the potential for local crack initiation, thereby enhancing the alloy's plasticity and processability[41–42]. However, as the rare earth content increases beyond ratio of 1: 1, the continuity and enrichment of the precipitate phases are gradually intensified. Modifications in the quantity and dimensions of precipitated phases may complicate interactions during grain boundary migration and grain deformation, potentially making the alloy more brittle and harder, and thus resulting in minimal alteration in the mechanical properties that should be enhanced by grain refinement.

Each group of as-cast alloys was subjected to solution treatment at 540 °C for 1 h followed by artificial aging at 180 °C for 5 h. As shown in Fig.9, alloy Z2, with Al-Ti-B:RE ratio of 3: 1, exhibits poor uniformity in the precipitation of secondary phases and the modification of Fe-rich phases. In contrast, alloy Z3, with Al-Ti-B: RE ratio of 2: 1, features precipitates that are smaller and more uniformly distributed throughout the matrix. This alloy displays numerous dot-like and particulate precipitates which may be Mg-Si strengthening phases, and no significant large-sized inclusions appear. For the alloy with a composite addition ratio of Al-Ti-

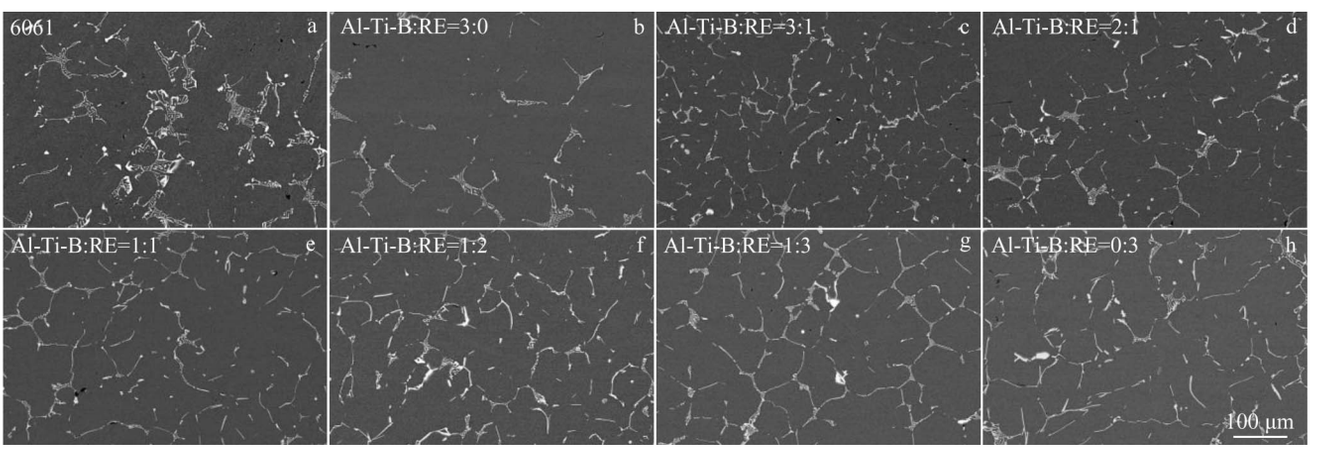

Fig.8 BSE images of original 6061 alloy (a) and modified as-cast alloys with different Al-Ti-B: RE ratios (b – h) after homogenization heat treatment: (b) 3:0, (c) 3:1, (d) 2:1, (e) 1:1, (f) 1:2, (g) 1:3, and (h) 0:3

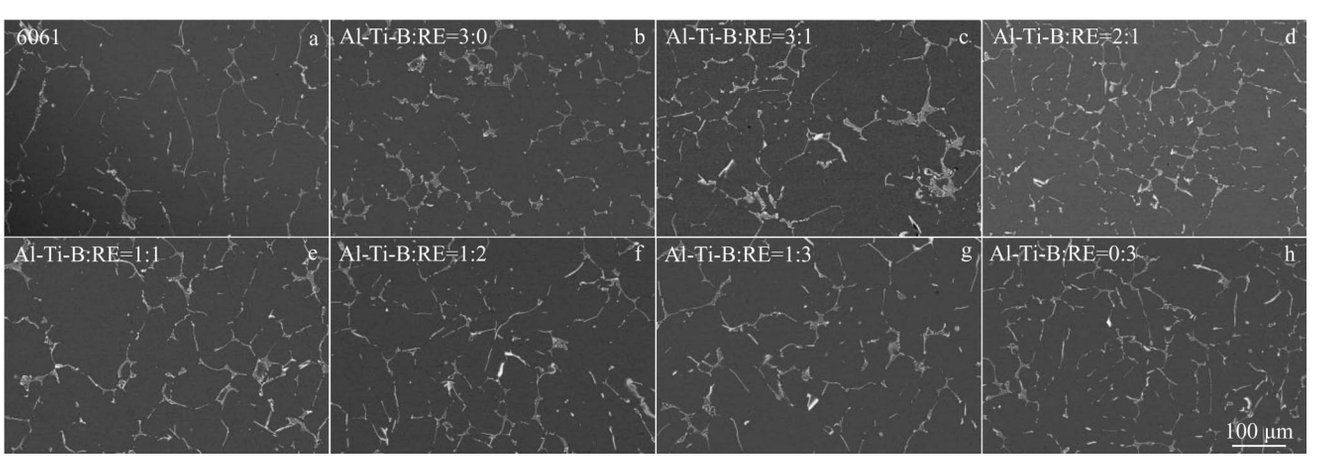

Fig.9 BSE images of original 6061 alloy (a) and modified as-cast alloys with different Al-Ti-B:RE ratios (b–h) after solid solution and aging heat treatment: (b) 3:0, (c) 3:1, (d) 2:1, (e) 1:1, (f) 1:2, (g) 1:3, and (h) 0:3

B:RE at 1:1, noticeable regions devoid of precipitates are still present, which can be attributed to either uneven grain structure or non-uniform aging precipitation. For the alloys with a higher proportion of rare earths, namely Z5, Z6 and Z7, there is a gradual increase in the number of feather-like or flake-shaped bright white inclusions. These findings highlight the complex interplay between alloying elements and microstructural evolution, significantly affecting the mechanical properties and processability of the alloys.

The types and elemental compositions of precipitate phases in various alloy groups were determined by energy dispersive spectroscopy (EDS). As shown in Fig.10a, in the alloy without rare earth element addition, the light gray dendritic Fe-rich phase is identified as AlFeSi(Mn), and dispersed granular phases AlFeSi(CuMg) are also present. Spherical precipitates, also in a dispersed state, are identified as Mg-Si phases containing a trace amount of Cu. In alloys with rare earth element additions, the AlFeSi(Mn) phases are refined, and rare earth-enriched precipitates appear predominantly as bright white feather-like, needle-like or spherical in form. According to EDS mapping and point analysis results (Fig. 11a) and combining XRD characterization results that show no shift in the Mg_2Si phase peaks, indicating stability of the crystal structure, and exhibit a decrease in peak intensity with increasing the concentrations of rare earth elements, it can be inferred that the spherical and acicular rare earth compounds likely form through partial adsorption of Ce and La elements on the original Mg-Si phase surfaces, leading to

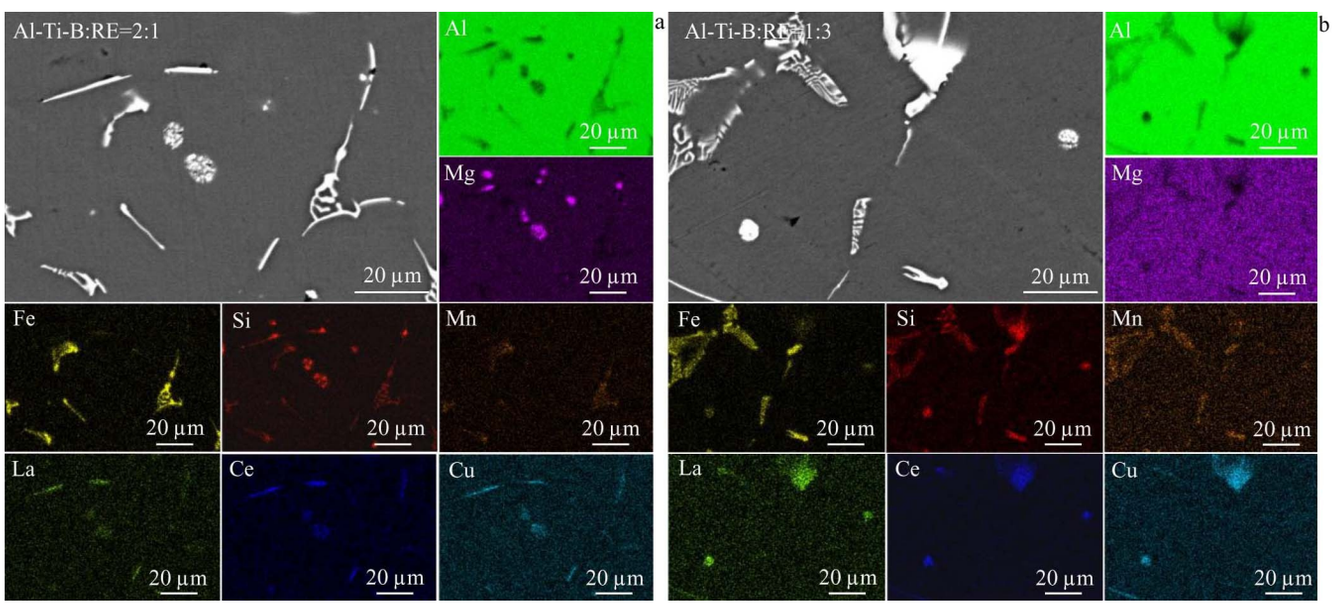

Fig.10 Microstructures and corresponding EDS mappings of alloys modified with composite additions of Al-Ti-B and rare earth element in ratios of 2:1 (a) and 1:3 (b)

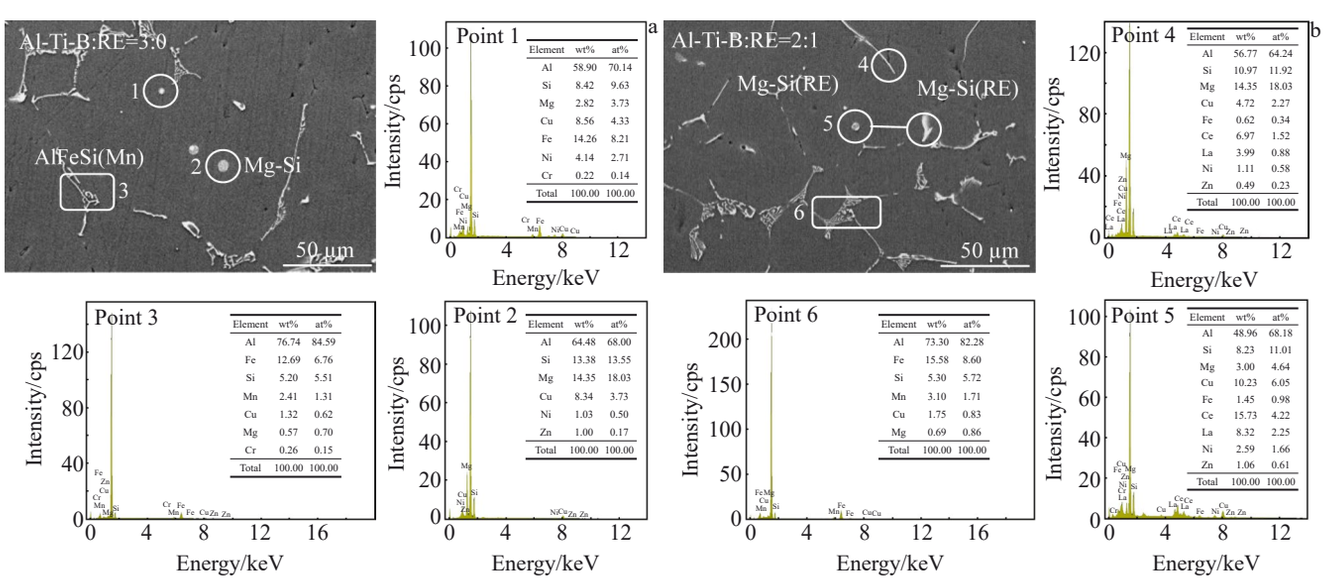

Fig.11 Microstructures and EDS point analysis results of as-cast alloys modified with individual Al-Ti-B (a) and composite additions of Al-Ti-B and rare earth element (b)

encapsulation[35]. Additionally, some rare earth elements preferentially bind and sequester Si atoms, resulting in the formation of phases such as AlLaSi and $CeCu_2Si_2$. The sequestration leads to a reduction in the Mg_2Si strengthening phase, potentially compromising the mechanical properties of the material. According to Fig. 11b, EDS point analysis of flake-like and granular rare earth phases indicates their composition as AlSiCuMg(CeLa)Fe. Comparing the precipitate morphologies and elemental composition in the alloys without rare earth element addition, it can be inferred that these rare earth compounds are complex combinations of Ce/La with Al, Si, Cu and other elements, or mixture of various rare earth compounds. Their volume and number increase with increasing the content of rare earth elements. While small numbers of these rare earth compounds can promote compositional undercooling and improve the coarse β -Fe phases, and excessively large rare earth compounds may act as sources of cracks, potentially compromising the toughness and strength of the alloys. This phenomenon may also contribute to the decreased plasticity observed in the as-cast and homogenized Z5, Z6 and Z7 alloys as the rare earth content increases.

Fracture surfaces of as-cast alloy tensile samples are illustrated in Fig. 12, revealing some inherent microstructure inhomogeneity within the as-cast alloys[43]. On the fracture surface of the original 6061 aluminum alloy, distinct cleavage planes and step features are observed, along with notable river patterns, which results from the movement of helical dislocations at the crack front. A closer examination of the scanned images reveals intergranular fracture characteristics, likely due to the enrichment of Fe-rich phases at the grain boundaries, corroborating the typical low plasticity of the as-cast original 6061 aluminum alloy. After the addition of Al-Ti-B into the alloy, although intergranular fracture characteristics are still observable on the fracture surfaces, larger dimples are also present. According to EDS element

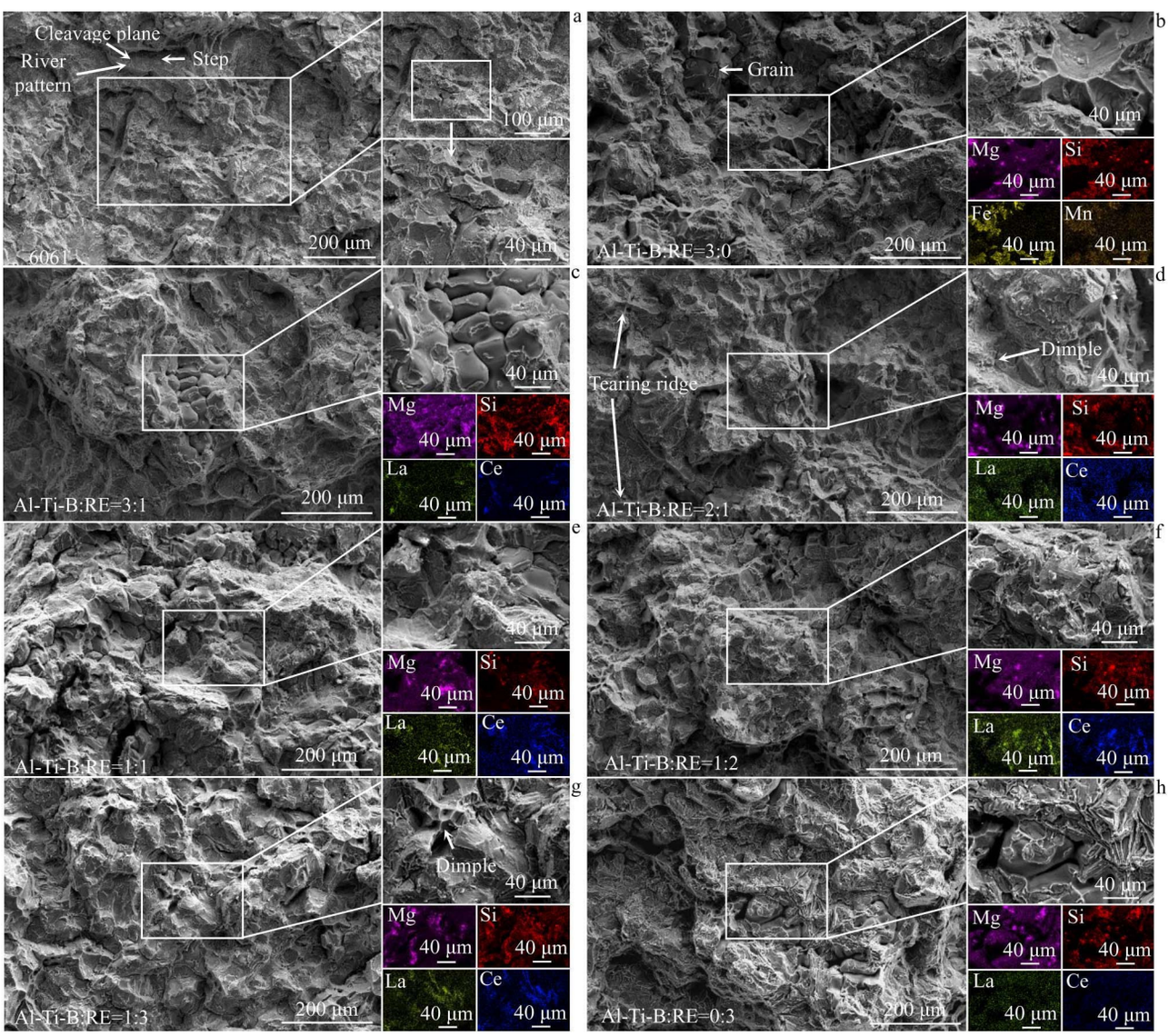

Fig.12 SEM images of fracture surface and corresponding EDS element mappings of as-cast alloy tensile samples: (a) Z0, (b) Z1, (c) Z2, (d) Z3, (e) Z4, (f) Z5, (g) Z6, and (h) Z7

mappings, it can be found that Mg-Si phase particles are found within the centers of dimples, contributing to the enhanced strength of the alloy. With the introduction of rare earth elements, especially at an Al-Ti-B:RE ratio of 2:1, more dimples are observable on the fracture surfaces, and some dimples are quite small. For these individual fine dimples, the force applied to the sample creates crack sources, which are propagated selectively and impeded upon reaching the grain boundaries, leading to improvements in both strength and elongation. Furthermore, the continuous addition of rare earths causes increasingly evident tearing features along the edges of intergranular fractures, which can positively affect the plasticity of the alloy to a certain extent. However, some positions enriched with Ce and La elements also contain traces of Si, suggesting that excessive rare earth (>0.1wt%) may destabilize the Mg-Si phase, thereby causing fluctuations in the mechanical properties of the alloy. The presence of larger rare earth phases can also lead to reduced ductility and toughness of the alloy.

2.5 TEM analysis

In this experiment, alloy Z3, with an optimal composite addition ratio of Al-Ti-B:RE=2:1, was selected as the representative sample for characterization. Initial morphological observations and EDS analysis are conducted on the bright needle-like precipitates that may contain rare earth elements within the Mg-Si phase, as previously identified by SEM characterizations of alloy Z3. From Fig. 13a and 13b, it is evident that the precipitates are composed of two distinct segments: dark-colored elongated needles closely associated with bright white needle-like phases. EDS mapping analysis of precipitates reveals that the dark region is Mg-Si phase, while the intermediate bright region is enriched with Ce, La and Cu alongside Si. The existence of distinct boundary between the two segments suggests that the typical long needle-like precipitation phases containing Ce, La, Mg and Si elements observed by SEM in the previous section should exist in the form of two distinct precipitation phases, rather than a single phase. Further EDS point analysis on the dark and bright sections indicates that the atomic ratio of Mg to Si within the Mg-Si phase is approximately 49.59% to 26.77% (nearly 2:1), and the atomic ratios of Cu, Si and Ce in the enriched zone are approximately 17.70%: 18.63%: 8.85% (roughly 2:2:1). Selected area electron diffraction (SAED) patterns of the interface of the dark and bright phases are corresponding to Mg_2Si and $CeCu_2Si_2$, respectively. The lattice parameters of $CeCu_2Si_2$ are notably similar to that of $Cu_2La_{0.5}Ce_{0.5}Si_2$, suggesting coexistence of these phases in the observed needle-like morphologies. Given the electronegativities of Mg (1.31), Si (1.90), Cu (1.90), Fe (1.83), Ce (1.12) and La (1.1), the polarity of bonds between Ce and La with Si is higher than that between Mg and Si, suggesting a stronger chemical bonding, which favors the formation of $CeCu_2Si_2$ due to similar differences in electronegativity between Cu/Si and Ce/La. Combining TEM findings with SEM and XRD results, it appears that excessive addition of rare earth elements can potentially lead to a significant consumption of Si to form larger rare earth phases. This might reduce the quantity of Mg_2Si strengthening phase, adversely impacting the mechanical properties of the alloy.

Furthermore, a portion of the rare earth phase is distributed in proximity to the Fe-rich phase, or more accurately, attached to the α-Fe phase, which also exhibits a needle and bar morphology, as shown in Fig. 14. Its elemental composition is found to be largely consistent with that of the aforementioned rare earth phase. The collective morphology of the rare-earth and α-Fe phase aggregates indicates that these mixed precipitates are analogous to the globular, RE-enriched and Fe-rich phases, as observed by SEM. Based on EDS results and analysis of electronegativities, it can be found that Ce and La elements interact with Si within the Fe-rich phases to form a new phase, $CeCu_2Si_2$. The interaction of rare earth elements with Si atoms in the Fe-rich phases alters their morphology,

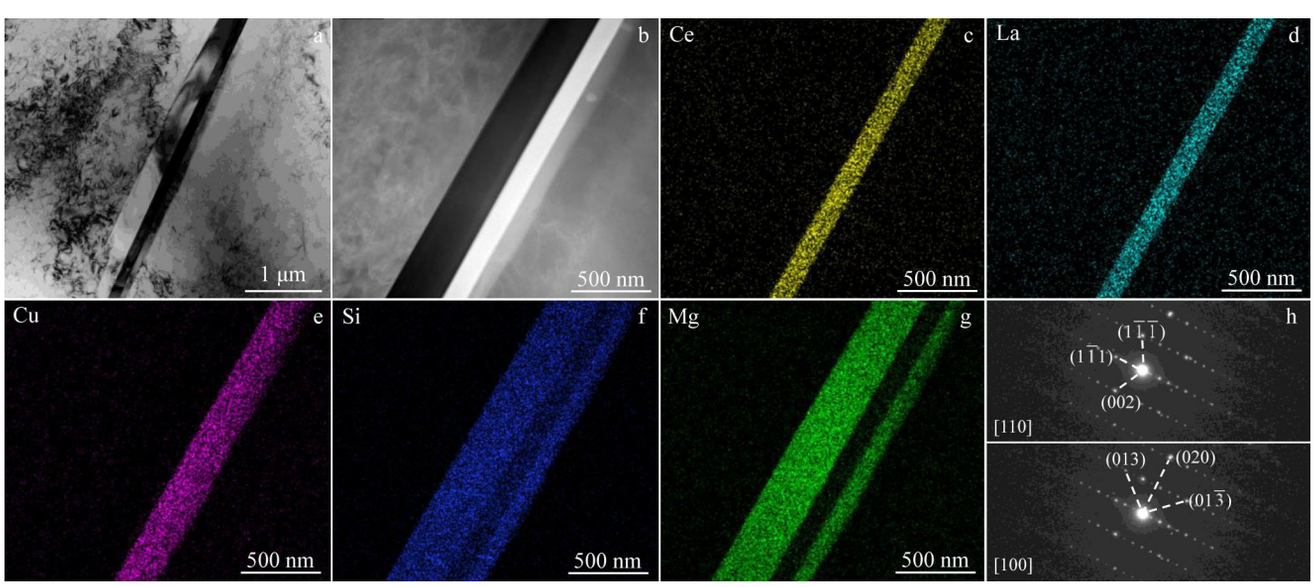

Fig.13 TEM images (a–b) with corresponding EDS element mappings (c–g) and SAED patterns (h) of precipitated phase in alloy Z3

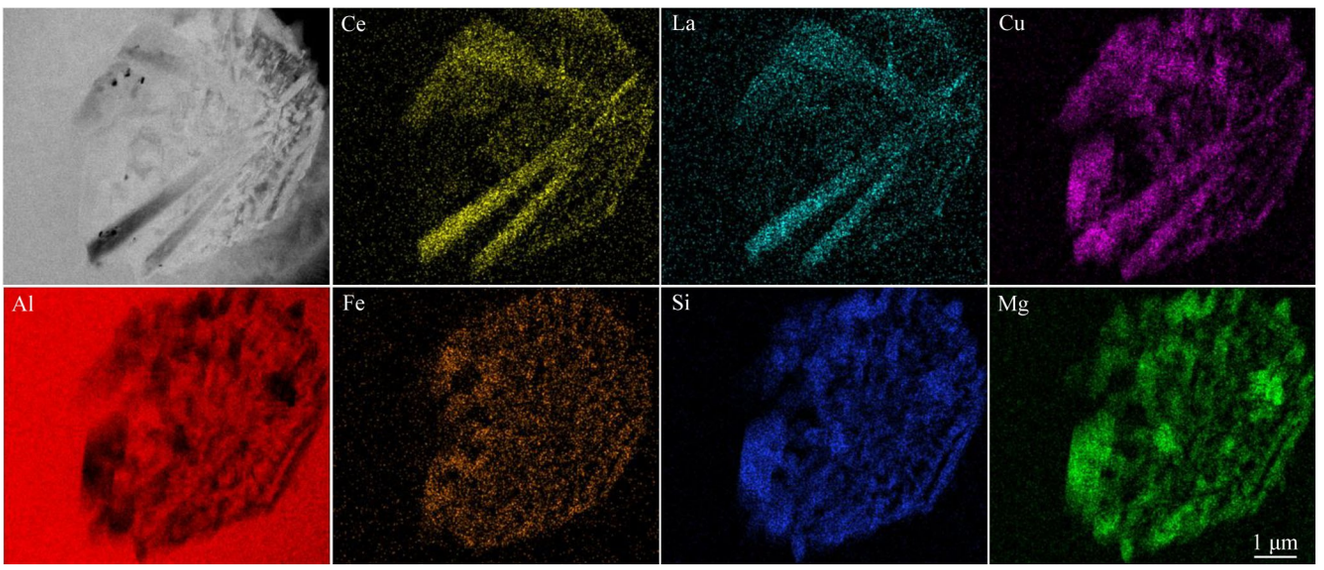

Fig.14 TEM image and corresponding EDS element mappings of precipitated phase in alloy Z3

whereby a small quantity of Ce and La can transform larger, elongated β-Fe phases into discontinuously distributed smaller Fe-rich phases or spherical α-Fe phases. This transformation reduces the embrittling and hardening effects associated with Fe-rich phases. Conversely, excessive concentration of rare earth elements, which leads to the formation of large rare earth phases, can also adversely affect the microstructural properties of the alloy, compromising its overall mechanical performance.

3 Conclusions

1) Incorporating cerium-rich rare earth elements with Al-Ti-B into the 6061 aluminum alloy, at a total addition level of 0.3wt% and in appropriate ratios, can effectively refine the grain structure of the alloy. The addition can also reduce the size of elongated β-Fe phases or transform them into spherical α-Fe phases. Such modifications significantly enhance the morphology of the precipitated phases, contributing to the overall improvement of the microstructural characteristics of the alloy.

2) When cerium-rich rare earths and Al-Ti-B are co-added to 6061 aluminum alloy, if the ratio of Ce to La elements is excessively high, specifically, if the proportion of rare earth elements exceeds a ratio of Al-Ti-B:RE=1:1 and the rare earth content surpasses 0.15wt%, several detrimental effects may occur. Firstly, Ce and La tend to react with Si atoms, forming an abundance of rare earth phases such as $CeCu_2Si_2$, which results in a reduction of the Mg_2Si strengthening phase. Secondly, the composition modification facilitates the growth of large rare earth phases within the alloy microstructure, which can act as potential new sources of cracks. This ultimately compromises the mechanical property of the alloy.

3) Upon the incorporation of cerium-rich rare earths and Al-Ti-B into the 6061 aluminum alloy at a ratio of 2:1 and a total addition of 0.3wt%, the fabricated alloy Z3 exhibits markedly enhanced ductility while retaining its inherent strength. Notably, the elongation of the Z3 alloy in its as-cast state exhibits a 50% increment relative to that of the original 6061 aluminum alloy. This substantial improvement in elongation underscores the efficacy of strategic additions of rare earths and Al-Ti-B in optimizing the mechanical properties of aluminum alloys.

References

1 Li H, Yan Z, Cao L. *Materials Science and Engineering A*[J], 2018, 728: 88
2 Zhang W, Xu J. *Materials & Design*[J], 2022, 221: 110994
3 Georgantzia E, Gkantou M, Kamaris G S. *Engineering Structures*[J], 2021, 227: 111372
4 Abdel-Hamid A A. *International Journal of Materials Research*[J], 1989, 80(8): 566
5 Johnsson M. *International Journal of Materials Research*[J], 1994, 85(11): 786
6 Qiu D, Taylor J A, Zhang M X. *Metallurgical and Materials Transactions A*[J], 2010, 41(13): 3412
7 Wang K Y, Zhao R D, Wu F F *et al. Journal of Alloys and Compounds*[J], 2020, 813: 152178
8 Wei B, Pan S, Liao G *et al. Materials & Design*[J], 2022, 218: 110699
9 Wang S B, Pan C F, Wei B *et al. Journal of Materials Science & Technology*[J], 2022, 110: 216
10 Zheng D, Li J, Wei B *et al. Journal of Materials Research and Technology*[J], 2023, 27: 472
11 Wang M, Wei W, Shi W *et al. Journal of Materials Research and Technology*[J], 2023, 22: 947
12 Cao P, Zhu D, Wu N *et al. Journal of Materials Research and Technology*[J], 2024, 29: 1359
13 Wang Xiaobo, Rong Li, Huang Hui *et al. Rare Metal Materials*

and Engineering[J], 2024, 53(1): 250 (in Chinese)
14 Fang W Q, Shen J R, Yan J K *et al. Rare Metal Materials and Engineering*[J], 2023, 52(7): 2326
15 Wu Y, Xiong J, Lai R *et al. Journal of Alloys and Compounds*[J], 2009, 475(1): 332
16 Jin H, Sui Y, Yang Y *et al. Journal of Materials Research and Technology*[J], 2022, 19: 1798
17 Lv Q, Zhang F, Wei H *et al. Vacuum*[J], 2023, 215: 112333
18 Mahmoud M G, Mosleh A O, Mohamed M S *et al. Journal of Alloys and Compounds*[J], 2023, 948: 169805
19 Ding W, Zhao X, Chen T *et al. Journal of Alloys and Compounds*[J], 2020, 830: 154685
20 Ding W, Cheng Y, Zhao X *et al. Materials Research Express*[J], 2020, 7(8): 86510
21 Chen Z Q, Hu W X, Shi L *et al. Foundry Technology*[J], 2022, 43(10): 897 (in Chinese)
22 Meng C, Tang H, Wang C *et al. Journal of Materials Research and Technology*[J], 2024, 30: 2420
23 Hosseinifar M, Malakhov D V. *Journal of Materials Science*[J], 2008, 43(22): 7157
24 Zhang Y, Wei F, Mao J *et al. Materials Characterization*[J], 2019, 158: 109963
25 Li D, Cai S, Gu J *et al. Materials Today Communications*[J], 2023, 36: 106666
26 Edwards G A, Stiller K, Dunlop G L *et al. Acta Materialia*[J], 1998, 46(11): 3893
27 Fang X, Song M, Li K *et al. Journal of Mining and Metallurgy, Section B: Metallurgy*[J], 2010, 46(2): 171
28 Maisonnette D, Suery M, Nelias D *et al. Materials Science and Engineering A*[J], 2011, 528(6): 2718
29 Bartawi E H, Marioara C D, Shaban G *et al. ACS Nano*[J], 2023, 17(23): 24115
30 Hosseinifar M, Malakhov D V. *Metallurgical and Materials Transactions A*[J], 2011, 42(3): 825
31 Yan L Z, Zhang Y A, Li X W *et al. Transactions of the Nonferrous Metals Society of China*[J], 2014, 24(4): 939
32 Zheng Q, Zhang L, Jiang H *et al. Journal of Materials Science and Technology*[J], 2020, 47: 142
33 Liao H, Liu Y, Lü C *et al. Journal of Materials Research*[J], 2017, 32(3): 566
34 Jiang H, Zheng Q, Song Y *et al. Materials Characterization*[J], 2022, 185: 111750
35 Zheng Q, Wu J, Jiang H *et al. Corrosion Science*[J], 2021, 179: 109113
36 Sisco K, Plotkowski A, Yang Y *et al. Scientific Reports*[J], 2021, 11(1): 6953
37 Kang M L, Deng Y L, Lei J Q *et al. Rare Metal Materials and Engineering*[J], 2024, 53(5): 1252
38 Yu Y, Pan Q, Wang W *et al. Journal of Materials Research and Technology*[J], 2021, 15: 6395
39 Wang W, Pan Q, Jiang F *et al. Journal of Alloys and Compounds*[J], 2022, 895: 162654
40 Mahmoud M G, Mosleh A O, Pozdniakov A V *et al. Journal of Alloys and Compounds*[J], 2022, 929: 167234
41 Kuijpers N C W, Vermolen F J, Vuik C *et al. Materials Science and Engineering A*[J], 2005, 394(1–2): 9
42 Li Q, Wang J, Liu X *et al. Materials Characterization*[J], 2024, 213: 114024
43 Xu Y X, Zhu M Z, Fang H C *et al. Rare Metal Materials and Engineering*[J], 2023, 52(10): 3556

富铈稀土和Al-Ti-B复合添加对Al-Mg-Si合金微观组织与力学性能的影响

种宇璠[1]，杜赵新[1]，巩天浩[1]，孙保安[2]，潘哲儒[1]，亓乐乐[1]，解程程[1]，程　军[3]
(1. 内蒙古工业大学 材料科学与工程学院，内蒙古 呼和浩特 010051)
(2. 中国科学院 物理研究所，北京 100190)
(3. 西北有色金属研究院，陕西 西安 710016)

摘　要：采用富铈稀土与Al-Ti-B直接复合添加的方式对6061铝合金进行改性。结果表明，适量Al-Ti-B与Ce、La元素按照一定比例添加时能够发挥协同作用促使合金晶粒细化。同时Ce、La元素与Si等元素结合形成稀土相，改善析出相的形态及分布，减弱β-Fe相对合金组织与力学性能的危害。当稀土含量过多时，一方面，本应该形成Mg_2Si相的一部分Si元素会被过多的Ce、La元素抢夺而导致强化相减少，另一方面，较多数量或较大尺寸的稀土相容易成为裂纹源，不利于合金组织的改善和性能的提升。富铈稀土与Al-Ti-B复合添加的形式能够在保证合金强度的同时显著提升6061铸态合金的塑性。采用复合添加比例为Al-Ti-B:RE=2:1时，制备得到的新型6061-RE铝合金在铸态状态下和经过均匀化热处理后，平均延伸率相较原始6061铝合金分别增长了50%与45%，这有利于合金后续的变形加工。采用复合添加比例为Al-Ti-B:RE=2:1时，制备得到的该6061-RE铝合金经540 ℃/1 h固溶与180 ℃/5 h时效热处理后，析出大量针状Mg-Si相，其平均极限抗拉伸强度与屈服强度分别达313.2与283.1 MPa，相较原始6061铝合金分别提升了12.3%与14.5%，平均延伸率提升了41%。

关键词：稀土合金；Al-Mg-Si合金；富铈稀土；力学性能；微观组织

作者简介：种宇璠，男，2000年生，硕士生，内蒙古工业大学材料科学与工程学院，内蒙古 呼和浩特 010051，E-mail：Cyf202002@126.com